Composites Part B 176 (2019) 107264

Contents lists available at ScienceDirect

Composites Part B

journal homepage: www.elsevier.com/locate/compositesb

Reactive toughening of intrinsic flame retardant urea-formaldehyde foam with polyether amine: Structure and elastic deformation mechanism

Yalong Liu, Lin Ye, Xiaowen Zhao *

State Key Laboratory of Polymer Materials Engineering, Polymer Research Institute of Sichuan University, Chengdu, 610065, China

ARTICLE INFO

Keywords:
Urea-formaldehyde (UF) foam
Polyether amine (PEA)
Cyclic compressive behavior
Elastic deformation mechanism
Intrinsic flame retardancy

ABSTRACT

Polyether amine (PEA) was chemically introduced onto urea-formaldehyde (UF) chains for the purpose of toughening UF foams via reactions of PEA involved hydroxymethylation and condensation in UF system. Through introduction of PEA component, the curing process of UF-b-PEA proceeded within a broader temperature range, and the curing peak shifted to a higher temperature. Compared with neat UF foam, UF-b-PEA foams exhibited polygonal open cells with larger cell size, longer strut length and higher open porosity. During cyclic compression, the Mullins effect and the area in the hysteresis loop were reduced for UF-b-PEA foam, indicating outstanding compression resilience and compressive stability of the foam. Due to the open-cellular structure of foam and excellent flexibility of PEA component, the critical force of Euler buckling (F_c) decreased obviously, indicating the deformability of UF-b-PEA foams was improved without fracture of strut during reversible deformation. Besides, UF-b-PEA foams showed outstanding flame retardancy.

1. Introduction

As a typical kind of thermosetting amino resin foam, urea-formaldehyde (UF) foam is manufactured through the environmental friendly water-based foaming process by the multifold reaction of the two monomers of urea and formaldehyde [1–4]. Due to the carbon/-nitrogen enriched structure, when UF foam burns, inert gases such as NH_3, CO_2 etc. are generated which can dilute oxygen, and meanwhile, a carbon layer forms to isolate the combustible gases and prevent the expansion of the flame. Thus, UF foam exhibits outstanding intrinsic flame retardancy and non-dripping during combustion [5,6], which is superior to that of widely used thermoplastic foams, such as polyurethane, polystyrene and polyethylene foam with low heat distortion point and high combustibility [7–15]. Moreover, UF foam possesses the advantages of low cost, so it has a promising future in the fields of building insulation, electronic appliances, chemical industry, and aerospace application [16]. However, due to the lack of flexible functional groups in UF molecules, UF foam suffers from high brittleness, high pulverization ratio and low strength, and thus, its applications are greatly restricted [17,18].

Liu et al. [19] prepared UF/polyacrylate molding compounds, and the impact strength was improved by 18% at 10 wt% polyacrylate content compared with that of the neat sample. Han et al. [20] studied the mechanical properties of polyethylene glycol toughened UF resin, and 16% improvement in impact strength was obtained for UF with 3 wt % polyethylene glycol. Also, in our previous study, polyurethane elastomers were chemically introduced into UF resin via in situ polymerization, and the toughness of UF resin can be clearly improved [21]. However, at present, few literatures are available on preparing elastic UF foams. Our group focused on the improvement of the elasticity of UF foam for several years and the previous work showed that, when high content of melamine (MA) component was chemically introduced into UF system via co-condensation reactions, the urea-melamine-formaldehyde (UMF) foam with a certain level of elastic compressive behaviour can be obtained [22].

Polyether amine (PEA) is a kind of polyalkylene oxide compound terminated with amino groups [23–25]. By adjusting the structure and degree of polymerization of the polyoxyalkylene chain of PEA, various performances such as reactivity, toughness, viscosity and hydrophilicity can be effectively regulated. In this work, PEA was chemically introduced into the UF system for the purpose of toughening UF foam. During the synthesis process, a large amount of terminal amino groups on the PEA chains can react with formaldehyde and further acetalization would occur. The C–O–C flexible structure on PEA chain was expected to endow UF foam with excellent toughness and UF-b-PEA foams with ultra-elasticity would be obtained. The effect of PEA content on the

* Corresponding author.
E-mail address: zhaoxiaowenscu@126.com (X. Zhao).

https://doi.org/10.1016/j.compositesb.2019.107264
Received 27 March 2019; Received in revised form 5 July 2019; Accepted 9 August 2019
Available online 9 August 2019

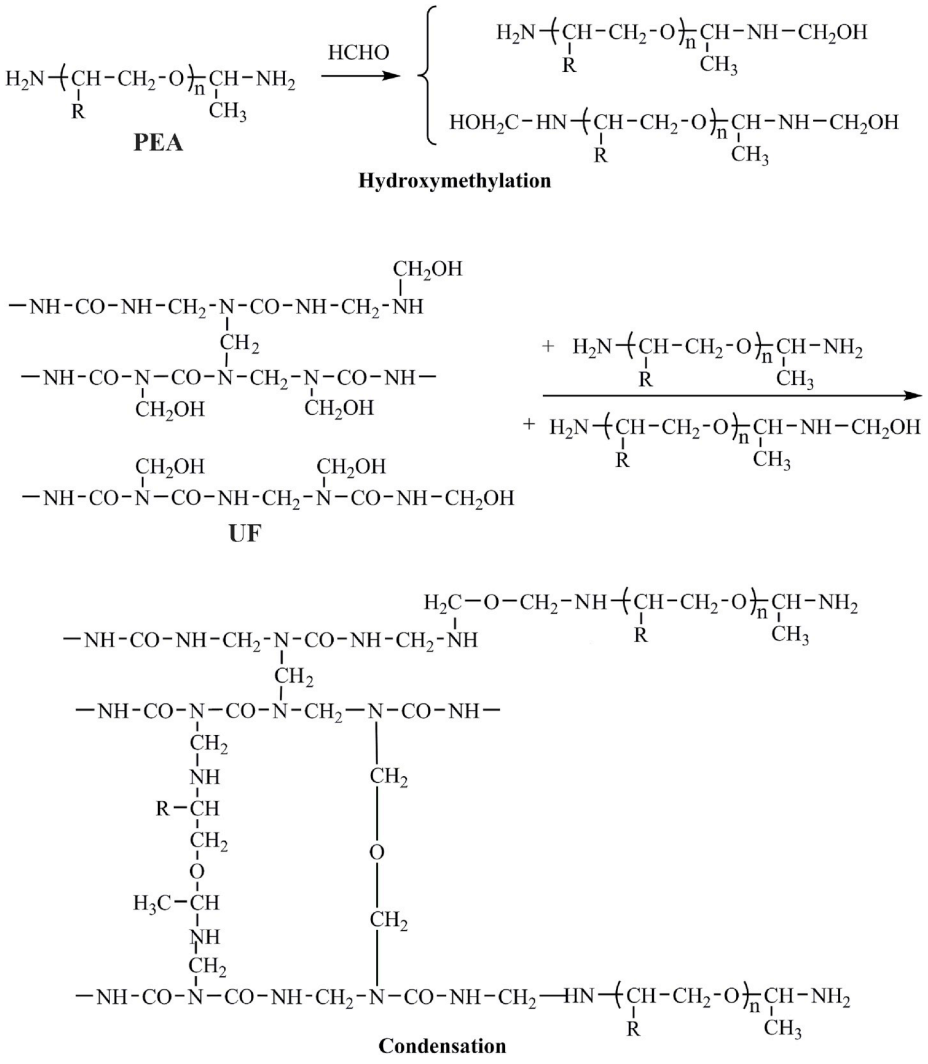

Fig. 1. PEA involved hydroxymethylation and condensation reactions in UF system.

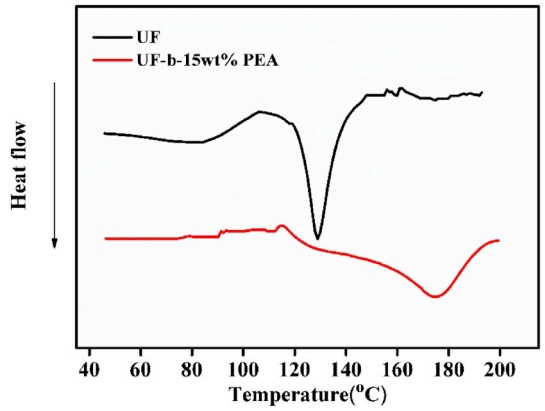

Fig. 2. DSC curves of neat UF and UF-b-PEA system during curing process.

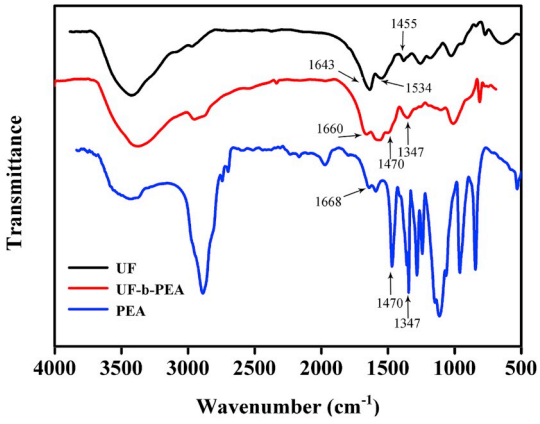

Fig. 3. FTIR spectrum of PEA, neat UF and UF-b-PEA system.

Table 1
Characteristic curing temperatures of neat UF and UF-b-PEA system.

Sample	Ti(°C)	T_p(°C)	T_e(°C)	Δw(°C)
UF	128.3	135.1	146.8	9.7
UF-b-15 wt%PEA	137.9	174.9	191.1	21.4

cellular structure, compressive mechanical behavior and flame retardancy of UF foam was studied. Moreover, the elastic deformation mechanism of UF-b-PEA foams was explored.

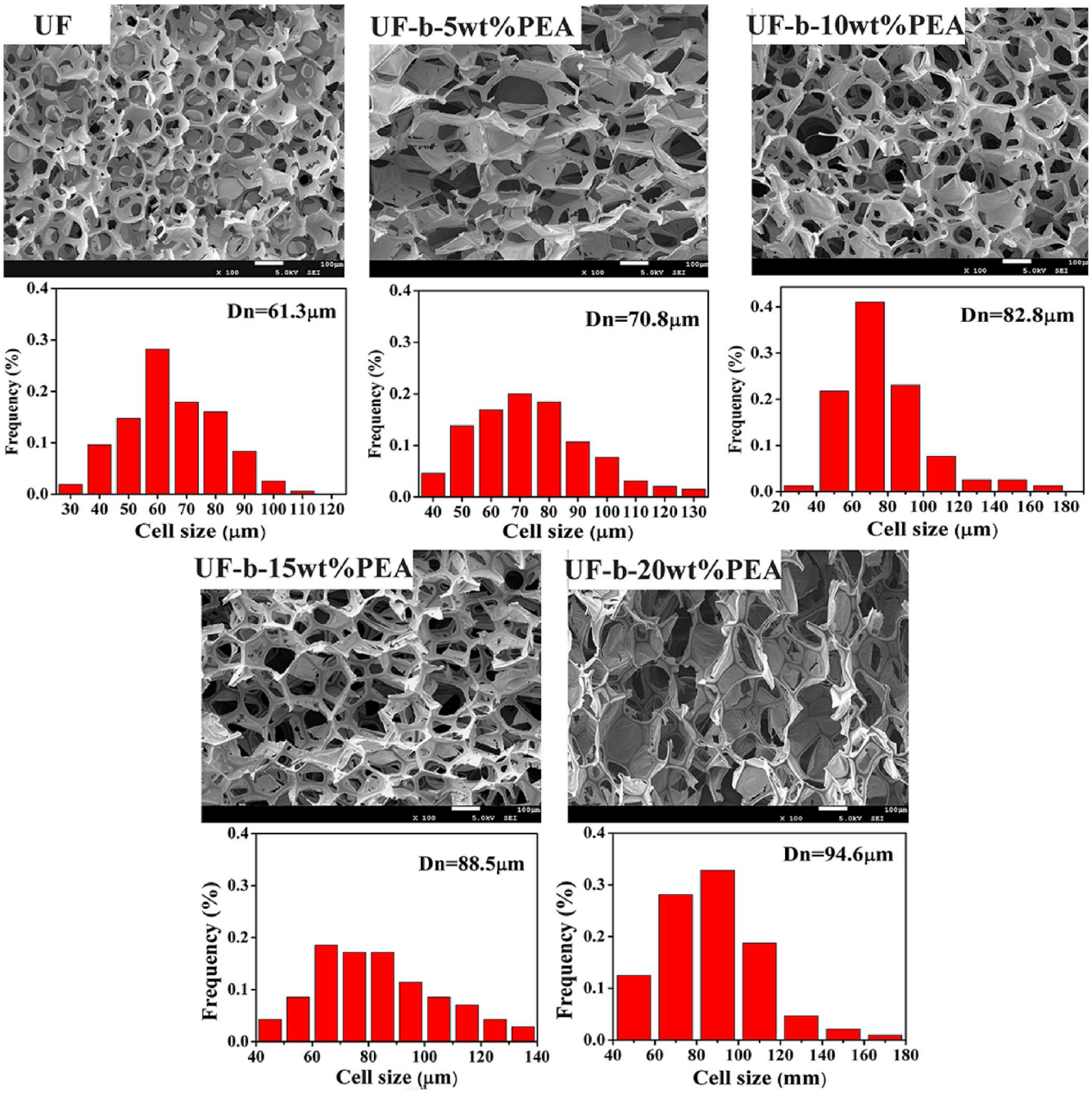

Fig. 4. SEM images and the corresponding cell size distribution of neat UF and UF-b-PEA foams.

2. Experimental

2.1. Materials

Urea was provided by Kelong Chemical Regents Co. Ltd (Chengdu, China). Formaldehyde water solution (37 wt%) as analytically pure reagents was purchased from Jinsan Chemical Reagent Co. Ltd (Chengdu, China). Sodium hydroxide (NaOH) was obtained from Xilong Chemical Co. Ltd (Chengdu, China). Formic acid, sodium dodecyl benzene sulfonate (SDBS) and pentane were all provided by Aike Chemical Regents Factory (Chengdu, China). Polyether amine with average molecular weights of 2000 g/mol and other chemical agents were all commercial grade products.

2.2. Synthesis and preparation

2.2.1. Synthesis of UF-b-PEA prepolymer resin

A proper quantity of PEA and formaldehyde were put into the reactor at 75 °C and maintained for 60 min. Then the first portion of urea was added and the mixture was adjusted to pH 7.8 with 10 mol/L NaOH aqueous solution, stirring for 50 min under medium speed. Subsequently, the system was adjusted to acidic conditions, and the second portion of urea was added. Finally, the system was adjusted to pH 7.8 again, and the resultant UF-PEA prepolymer resin was obtained. For comparison, neat UF prepolymer resin was synthesized with the same method.

2.2.2. Preparation of UF-b-PEA foam

At first, a certain quantity of emulsifier (SDBS) and foaming agent

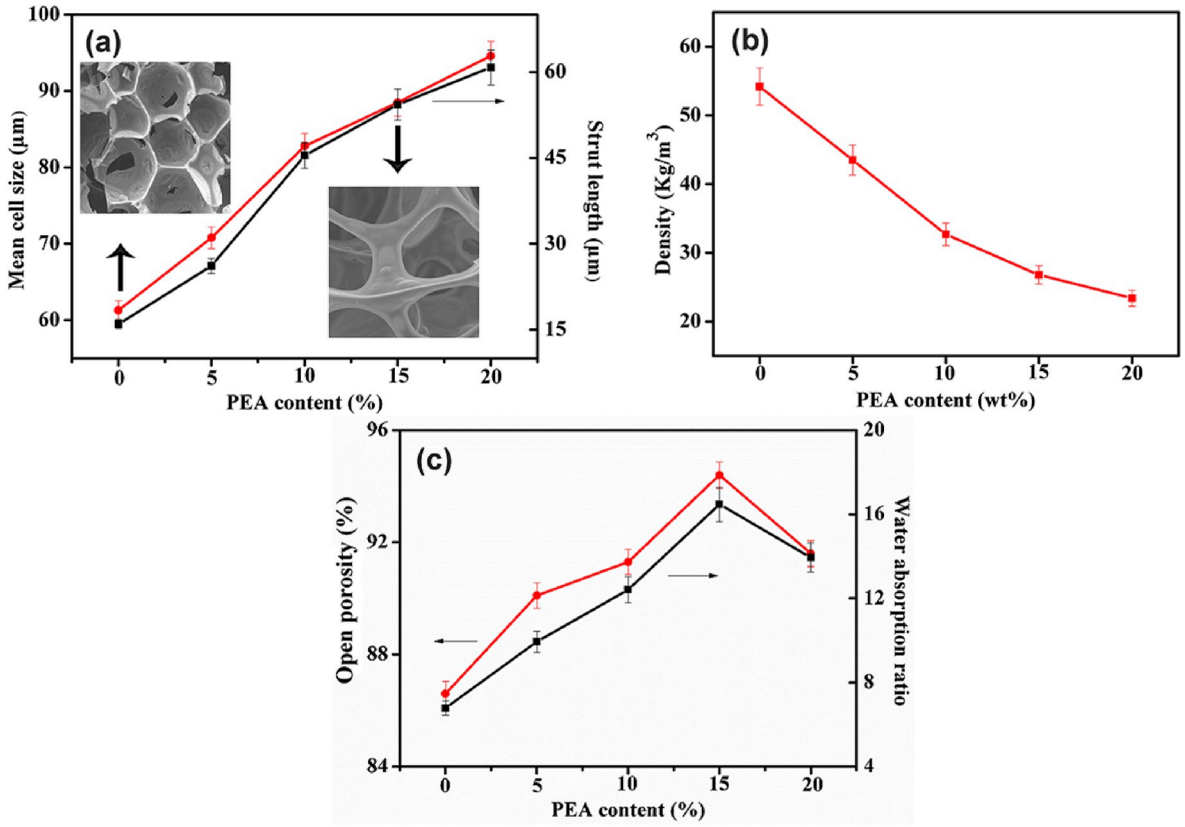

Fig. 5. The mean cell size and strut length (a), apparent density (b), open porosity and water absorption (c) of neat UF and UF-b-PEA foams.

(pentane) were dispersed in the prepolymer resin by a high-speed mechanical mixer. Then curing catalyst (formic acid) was added and stirred quickly for 40 s. Finally, the obtained viscous mixture was quickly poured into a foaming mould, and then cured and foamed in the oven.

2.3. Measurements

2.3.1. Differential scanning calorimetry (DSC) analysis

DSC curves of UF foams during curing were performed with a Netzsch 204 DSC instrument (Netzsch Co., Germany). The samples of about 5 mg were placed in a stainless steel crucible. The range of the test temperature was 20 °C–230 °C which was calibrated with indium.

2.3.2. Scanning electronic microscopy (SEM) analysis

The micro-porous morphology of UF foams was observed with a JSM-5900LV SEM (JEOL Ltd. Japan) under operating voltage of 5 kV. The samples were ion beam sputter-coated with gold and the thin layer thickness was about 1–20 nm. The cell size and its distribution were statistical analysed with Image Pro Plus 6.0 software [26,27].

2.3.3. Apparent density

The apparent density of UF foams was measured according to ISO 845:2006, and calculated as follows [28]:

$$\rho = m/v$$

where ρ is the apparent density ($kg{\cdot}m^{-3}$) of the sample; m is the mass (kg) and v is the volume of the sample (m^3). Samples with 50 × 50 mm in squares and 10 mm in thickness were prepared.

2.3.4. Water absorption and porosity

The water absorption of UF foams was investigated according to ISO 2896:2001. Samples with dimensions of 50 mm × 50 mm × 20 mm were dried in the oven for 2 h at first, and then were immersed into the distilled water for 24 h. Finally, samples were taken out and wiped to remove the excessive water on their surface. By measuring of the weight changes of the samples before and after immersion, the water absorption can be calculated as follows:

$$\text{Water absorption } (\%) = [(m_2\text{-}m_1)/m_1] \times 100\%$$

where m_1 is the mass of dry sample before immersion, and m_2 is the mass of foam after immersion in the water for 24 h.

The porosity of UF foams was also measured with an immersion method according to GB10799-2008, and determined with the following formula [29]:

$$Porosity = [(G_2 - G_1)/\rho]/[(G_2 - G_3 + G_4)/\rho] = [(G_2 - G_1)]/[(G_2 - G_3 + G_4)]$$

where G_1 is the weight of the dry foam in the air (before immersion); G_2 is the weight of saturated foam after immersion in the water for 24 h; G_3 is the total weight of the saturated foam and tray measured in the water; G_4 is the weight of the tray measured in the water; ρ is the density of water.

2.3.5. Compression properties

According to ISO 844:244, the compression properties of UF foams were carried out with a 4302 material testing machine (Instron Co., U.S. A.) [30]. Parallel tests were made at least five times.

2.3.6. Flame retardancy

The limiting oxygen index (LOI) was measured with a HC-2 oxygen index meter (Jiangning Analysis Instrument Co., China) according to ASTM D 2863-2008 [31]. Samples with dimensions of 100 mm × 10 mm × 10 mm were prepared.

The vertical burning test (UL-94) was performed on HK-HVRA instrument (Huake Co., China) according to ASTM D 3801 [32]. Samples with dimensions of 125 mm × 10 mm × 10 mm were prepared.

The flammability of UF foams was also investigated by a FTT cone

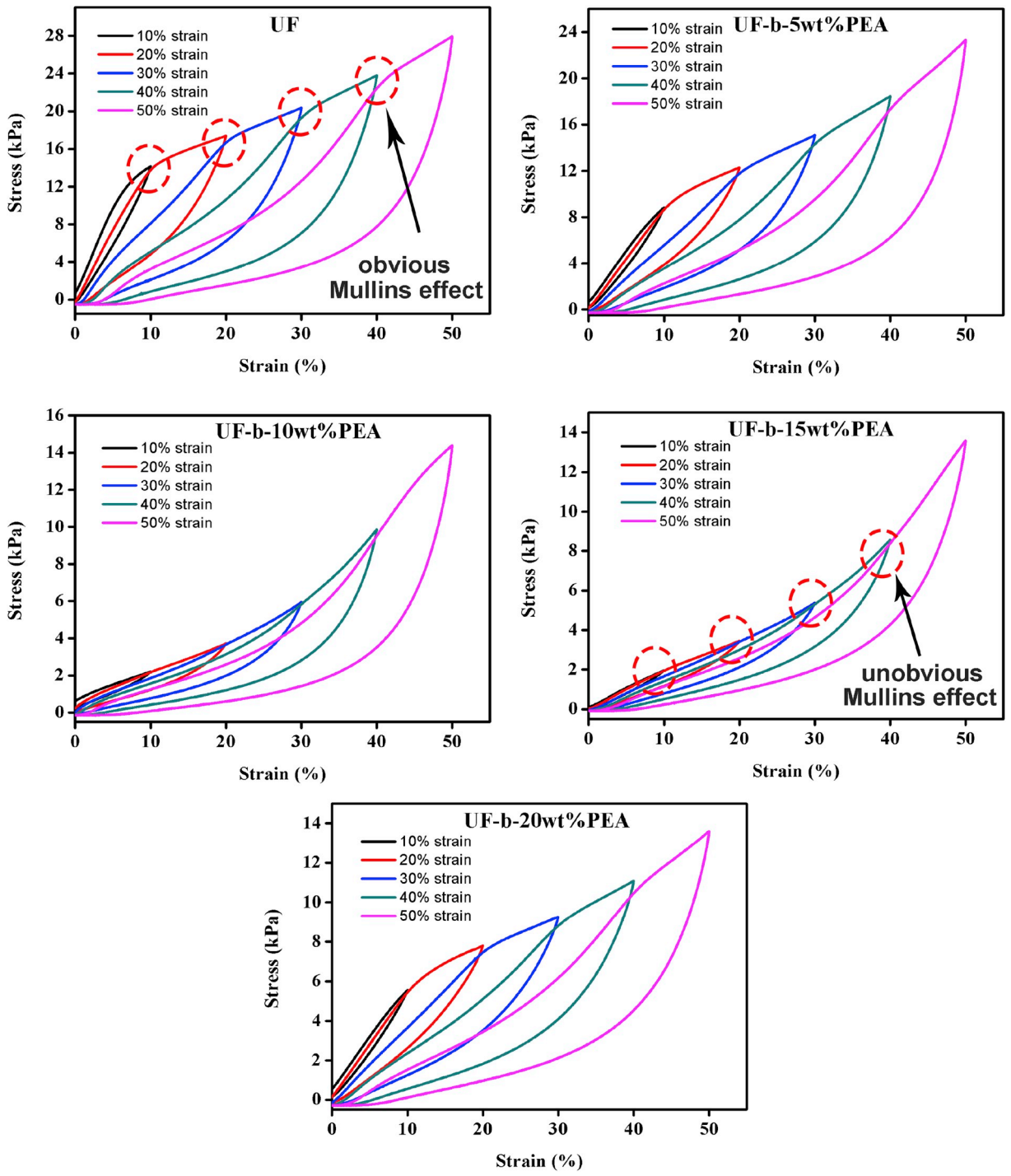

Fig. 6. Cyclic compression stress–strain curves of neat UF and UF-b-PEA foams with increasing strain amplitudes.

calorimeter (Fire Testing Technology, Ltd., U.K.) according to ISO-5660-1 under a heat flux of $50 \pm 1\ kW/m^2$. The samples were cut into 100 mm × 100 mm × 8 mm and wrapped in aluminum foil before the test.

3. Results and discussion

3.1. Preparation of UF-b-PEA foam

During the synthesis of UF-b-PEA resin, PEA was first mixed with formaldehyde to promote the reactions between them. Then, urea was added to the PEA-formaldehyde system to synthesis the UF-b-PEA resin via the traditional alkaline-acid-alkaline three-step reaction [33]. Finally, based on water-based foaming process, UF-b-PEA foams were prepared by using SDBS as emulsifiers, pentane as foaming agent and formic acid as curing agent. The reaction of PEA involved hydroxymethylation and condensation in UF system was shown in Fig. 1.

DSC analysis was used to study the effect of PEA component on the curing behavior of UF foam. DSC curves for neat UF and UF-b-15 wt% PEA resin during curing with heating rate of 10 °C/min were shown in Fig. 2 and the related data including initial temperature (T_i), end temperature (T_e), peak temperature (T_p) and half peak width (Δw) were listed in Table 1. As thermosetting resin, the curing reaction of UF was exothermal processes. For neat UF resin, the exothermic peak appearing

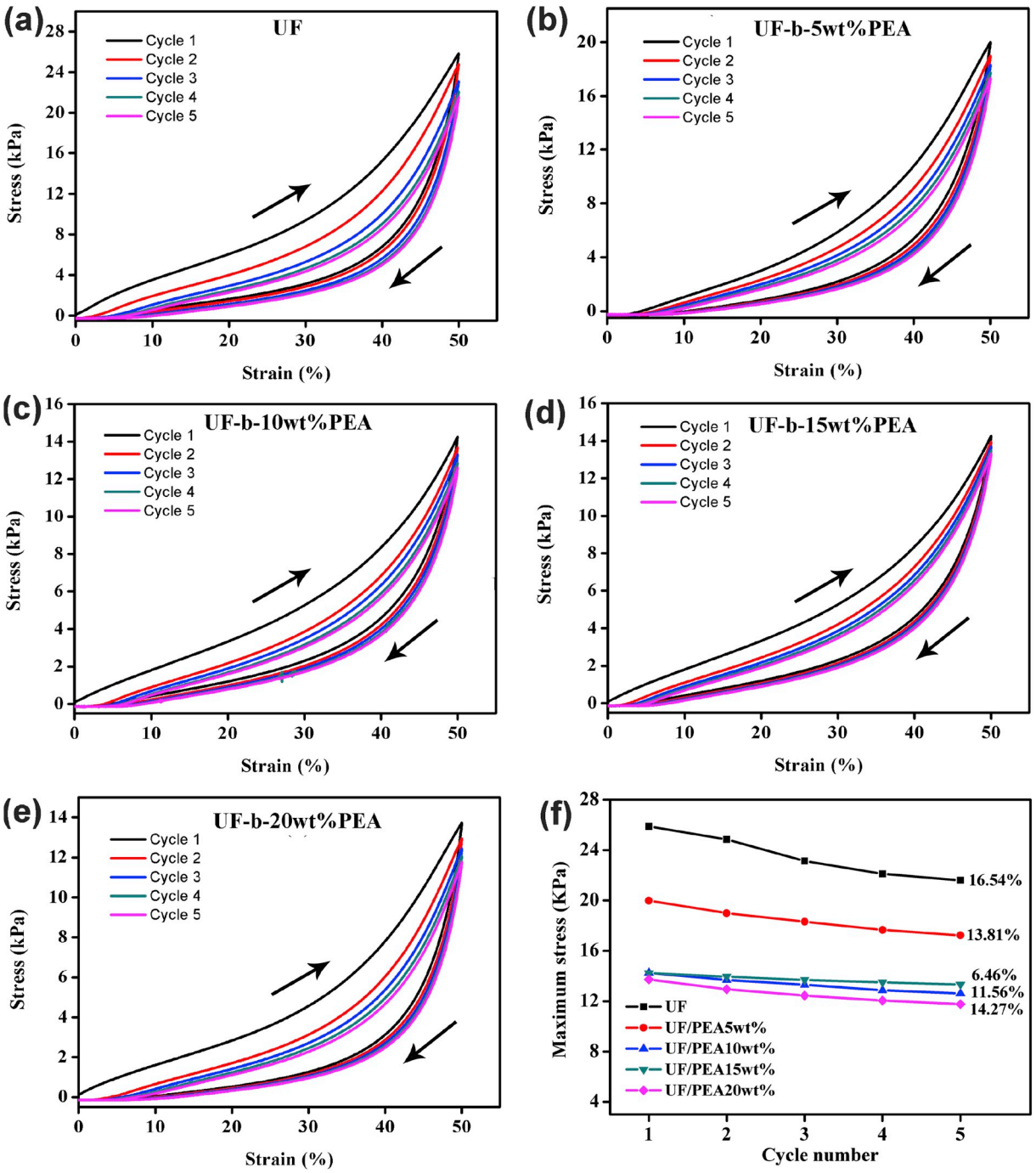

Fig. 7. Cyclic compression stress–strain curves up to a strain of 50% (ãe), stress versus cycle number at strain of 50% (f) for neat UF and UF-b-PEA foams.

at about 135.1 °C could be ascribed to the heat released from the polycondensation reaction between hydroxymethyl groups (–CH_2OH). Compared with neat UF foam, the curing process of UF-b-PEA proceeded within a broader temperature range, and the peak temperature shifted to a higher temperature of 174.9 °C, suggesting that, due to the relative low reactivity of PEA, high curing temperature was necessary for UF-b-PEA system and the curing process was prolonged.

The structural features of neat UF, PEA and UF-b-PEA samples were characterized by FTIR analysis, as shown in Fig. 3. For the neat UF foam, the characteristic absorption peak at 1640 cm^{-1} was attributed to the C═O asymmetric vibration. The absorption peaks at 1534 cm^{-1} and 1455 cm^{-1} were assigned to the –NH– bending vibration of the secondary amine group and the C–H stretching vibration of hydroxymethyl, respectively [34,35]. The absorption peak at 1030 cm^{-1} was assigned to the C–O stretching vibration of hydroxymethyl. For the PEA, the characteristic absorption peak at 1668 cm^{-1} was attributed to the N–H bending vibration of primary amine. The absorption peaks at 1470 cm^{-1} and 1347 cm^{-1} were assigned to the antisymmetric and the symmetric bending vibration of methyl group, respectively. For UF-b-PEA foam, besides the above mentioned characteristic absorption peaks of UF, the appearance of peaks at 1660 cm^{-1}, 1470 cm^{-1} and 1347 cm^{-1} attributed to the primary amine and methyl groups of PEA, indicated that PEA molecules were successfully introduced onto the UF molecular chains.

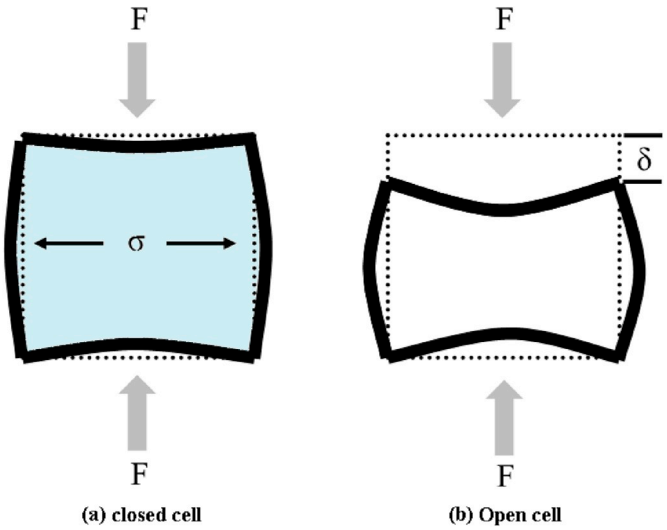

Fig. 8. Schematic representation of buckling of a cell face under the force.

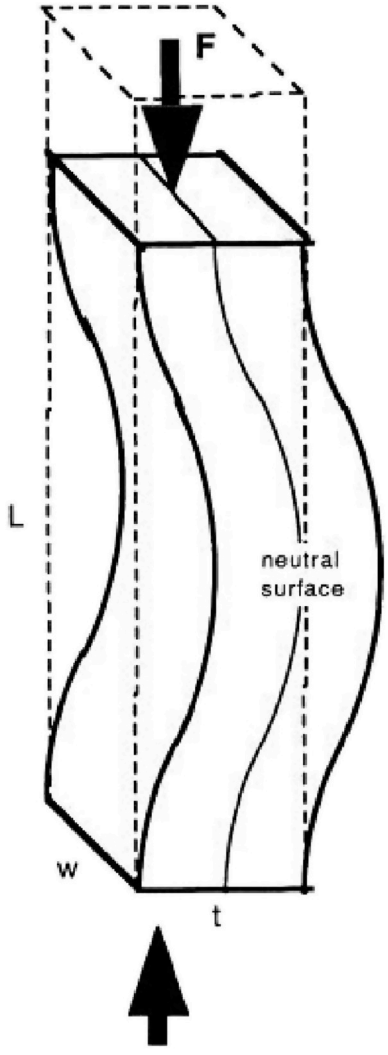

Fig. 9. Schematic representation of buckling of a cell strut under the force.

3.2. Cell morphology and apparent density of UF-b-PEA foam

The effect of PEA content on the microstructures such as cell size and its distribution was examined by SEM analysis. As shown in Fig. 4, the neat UF foam showed the semi-open cellular structure and the shape of the cell was almost spherical. For the UF-b-PEA foam with PEA content of 5–15 wt%, a large number of polygonal open cells with large cell size and thin cell walls can be observed. However, when the PEA content reached 20 wt%, the cell size became non-uniform and large voids appeared.

The mean cell size and strut length of the foams with various content of PEA were shown in Fig. 5(a). With the increase of PEA content, the mean cell size increased from 61.3 μm to 94.6 μm, while the strut length increased from 16.0 μm to 60.8 μm. It can be seen from DSC results that, the curing process of UF-b-PEA proceeded within a broader temperature ranges, and the peak temperature shifted to a higher temperature by the introduction of PEA, which indicated a decrease of the curing rate. Therefore, for UF-b-PEA foam, when the foaming rate kept constant, the combination of the adjacent cells were apt to occur during foaming process, and thus considerable open cells with large pore size and long struts formed.

The apparent density of UF-b-PEA foams with different PEA content was shown in Fig. 5(b). It can be evidently seen that the apparent density of foams gradually decreased with the increase of PEA content. The decrease in apparent density of foam was greatly related to the cell size and size distribution, which determines foam volume. The larger cell diameter led to lower apparent density of foams.

To verify the open-cell structure of UF-b-PEA foams, a convincing experiment was carried out by water absorption. Fig. 5(c) presented the water absorption and porosity of UF-b-PEA foams with different content of PEA. It can be seen that both the water absorption and porosity of the foam increased at first and then declined slightly with the increase of PEA content, which reached maximum at 15 wt% PEA content. The water absorption capability of foams was directly related to its open porosity and higher water absorption usually indicated the increase of open porosity.

3.3. Compressive behavior and elastic deformation mechanism of UF-b-PEA foam

3.3.1. Cyclic compressive behavior

Cyclic compression stress–strain curves of neat UF foam and UF-b-PEA foams with increasing strain amplitudes and a fixed strain rate were shown in Fig. 6. In the elastic deformation region, the neat UF foam showed higher compressive stress and modulus than that of UF-b-PEA foam; while the plateau region of UF-b-PEA foam was significantly broadened which could maintain stress in a wider strain range, indicating that UF-b-PEA foam showed a higher deformability before the cell structure was destroyed. In addition, during the compression cycle, the stress of neat UF foam at the unloading point was always higher than the stress required when reloading to the same strain. Namely when the same compressive strain was reached, the stress required for the first compression was the largest. Then during the subsequent four compression cycles, the stress value decreased gradually, showing a significant Mullins effect, which was mainly caused by the damage of the cell structure. However, it was notable that introduction of PEA could significantly reduce the Mullins effect of the foam. When the PEA content was 15 wt%, Mullins effect could be rarely observed in the stress-strain curve. When PEA content increased further and reached up to 20 wt%, Mullins effect became more obvious again.

Fig. 7(ãe) showed a set of load-unload stress-strain results up to a strain of about 50%. During cyclic compression, hysteresis can be observed for both neat UF foam and the UF-b-PEA foams, for which the unloading path displayed less stress than the loading path in the same cycle. The area under loading curve represented supplied energy while the area under downloading curve represented the recovered energy

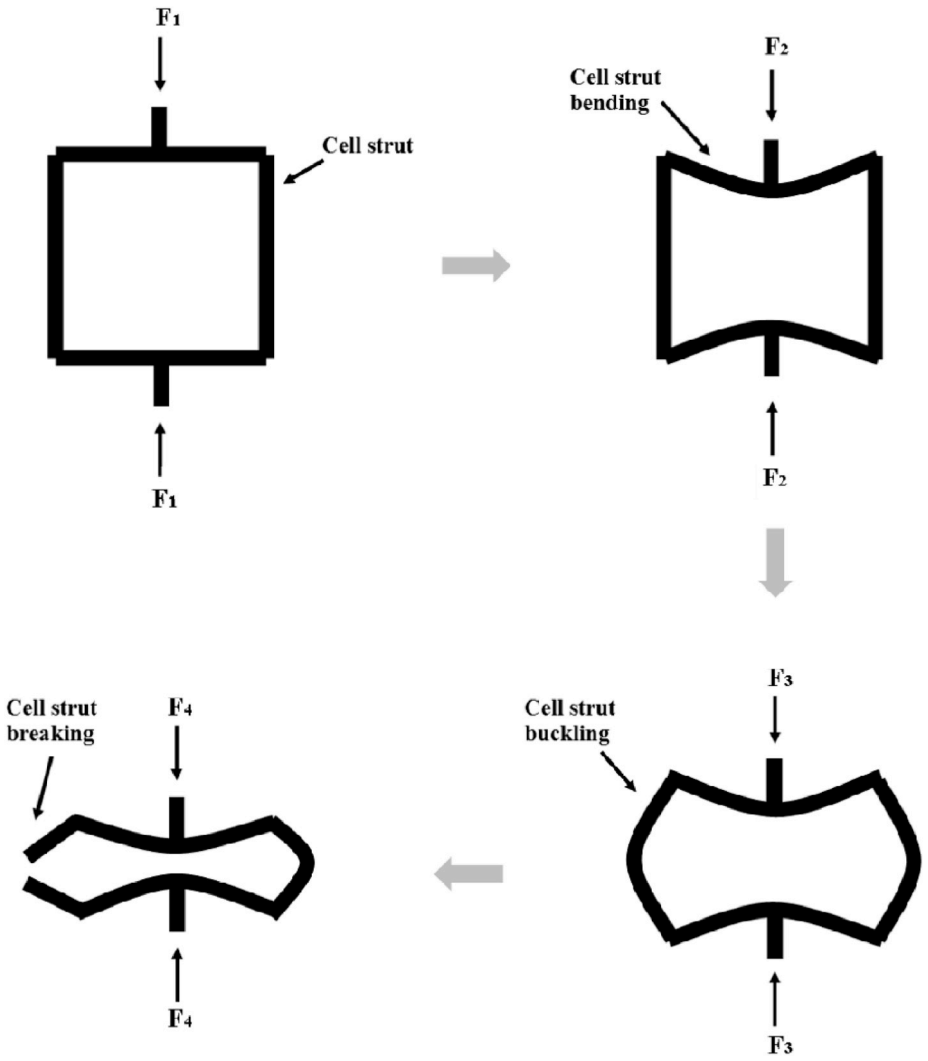

Fig. 10. Schematic representation of the deformation of cell struts under different level of compression ($F_4>F_3>F_2>F_1$).

upon unloading. Hence the area in the hysteresis loop represented dissipated energy [36,37]. As shown in Fig. 7(ãe), the neat UF foam displayed larger area in the hysteresis loop indicating more substantial mechanical damping. With the increase of PEA content, the compression cycle curves for UF-b-PEA foams showed better repeatability, indicating outstanding compression resilience of the foams.

Fig. 7(f) showed the relationship between the maximum compressive stress and the number of cycles at strain of 50%. The compressive stress of the neat UF foam decreased by 16.54% after five compressive cycles, while that value for UF-b-15 wt%PEA foam decreased by only 6.46%, indicating that UF-b-15 wt%PEA foam showed better compressive stability. However, for UF-b-20 wt%PEA sample, after five compressive cycles, a more obvious decline in compressive stress at strain of 50% can be observed. When the PEA content reached 20 wt%, the cell size became non-uniform and large voids appeared for the foam. Thus, during compression, the cracks can be initiated easily at the cell walls around the large voids and then propagated. Such damage of the cell structure lead to an irreversible deformation during compression, and thus a certain Mullins effect occurred.

3.3.2. *Elastic deformation mechanism*

The compressive behavior of the foam depended largely on its cell structure. As shown in Fig. 8(a), for neat UF foam with low open porosity, when a uniaxial force, F, was applied, the membranes which formed the cell faces would bend, while the cell edges began to bend or extend, increasing the contribution of the cell wall stiffness to the elastic moduli of the foam. Therefore, the deformation of neat UF foam occurred under a higher stress. However, for the UF-b-PEA foam with high open porosity, the deformation could occur primarily by strut bending, resulting in high deformability of the foam (as shown in Fig. 8 (b)).

For open cell foams, the compressive deformation is closely related to the characteristics of the struts themselves. Euler buckling [38] can occur when struts are compressed axially (as shown in Fig. 9), and the critical forces Fc was given by equation:

$$\mathrm{Fc} = \left(\frac{2\pi}{L}\right)^2 EI$$

where L is the length of strut; E is the Young's modulus of the material and I is the second moment of area of the strut cross-section.

With the increase of PEA content, the length of strut increased and the Young's modulus decreased. Therefore, the F_c decreased and the ability of deformation of the UF-b-PEA foams was improved.

The single cell model of the mechanical response of UF-b-PEA foam during loading was illustrated in Fig. 10. At low stress, the bending and buckling deformation of the foam came about through bending of the cell strut. By unloading, the cell could completely return to the original state. With the increase of stress, the bending and buckling deformation of cell struts were more obvious. When the load was greater than the

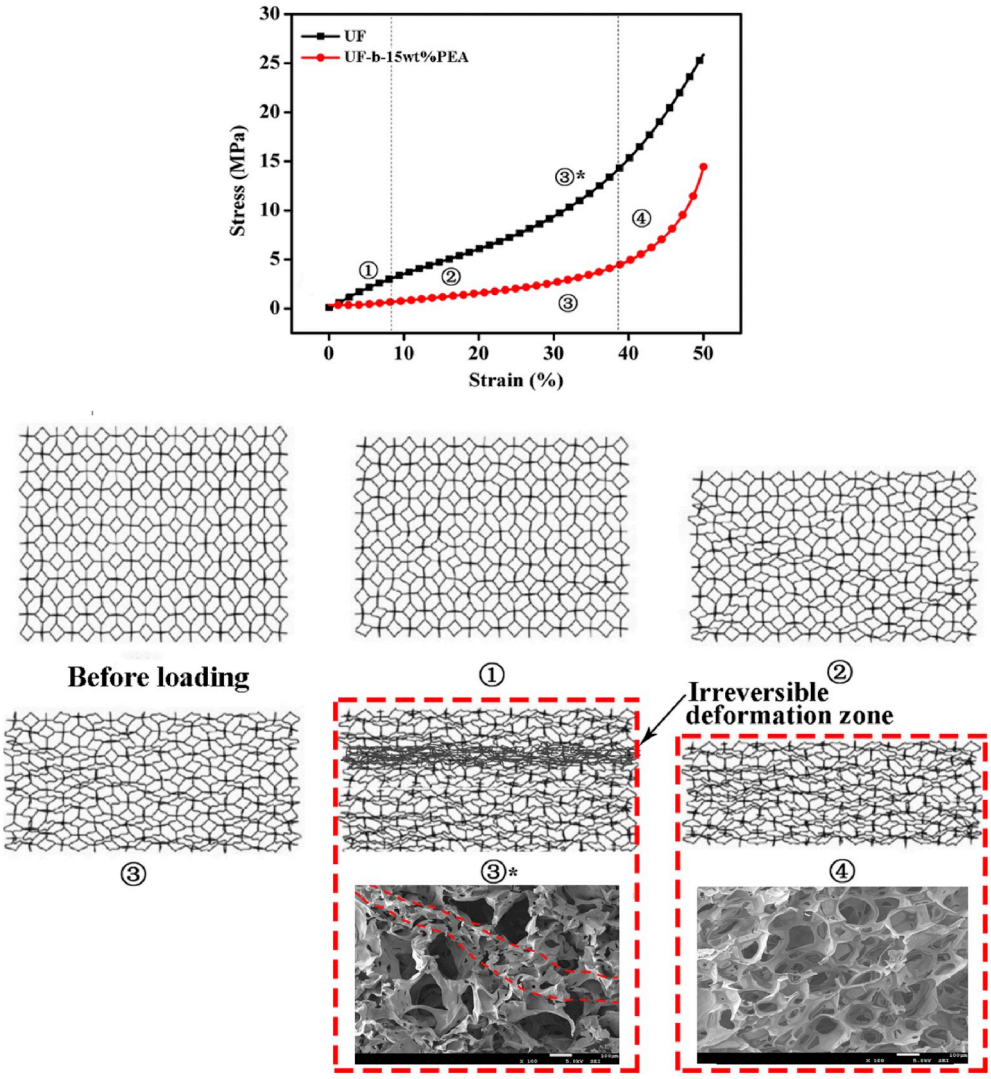

Fig. 11. Stress–strain curves and a series of deformed configurations of neat UF and UF-b-PEA foams during compression.

Table 2
LOI values and UL-94 classification of neat UF and UF-b-PEA foam.

Sample	LOI(%)	Vertical burning test rating
UF	35.5	V0
UF-b-5wt%PEA	34.7	V0
UF-b-10 wt%PEA	33.9	V0
UF-b-15 wt%PEA	33.2	V0
UF-b-20 wt%PEA	30.0	V0

stress that the cell strut could bear, the cell strut yielded and broke, and then the irreversible deformation occurred. With the increase of PEA content, the reversible deformation of foams increased, due to the increasing open porosity as well as strut length and the decreasing Fc. However, when the PEA content was 20 wt%, the cell strut could not bear larger loads, resulting in irreversible deformation of the cell.

Fig. 11 showed a set of deformed configurations of multiple cells corresponding to the different stages of the stress–strain curves (marked by numbers) for neat UF and UF-b-PEA foam. Before loading, no deformation of cells can be observed for all samples. For configuration ①, the foams were subjected to small load and the cell strut began to bend, while little change in foams shape could be observed on the macro level. With the increase of strain, the deformation of cells became obvious for the foams (as shown as configuration ②). For neat UF foam, the deformation

Fig. 12. Photographs of neat UF and UF-b-PEA foams after UL-94 test.

of cells was restrained by the cell walls and short cell strut, and thus it displayed high compression stress and modulus. For UF-b-PEA foam, because the deformation of cell strut and single cell were easier than that of neat UF foam, large cooperative deformation of cells can be produced (as shown as configuration ③). However, at the same strain for neat UF foam, the irreversible yielding and damage of strut and cell wall occurred

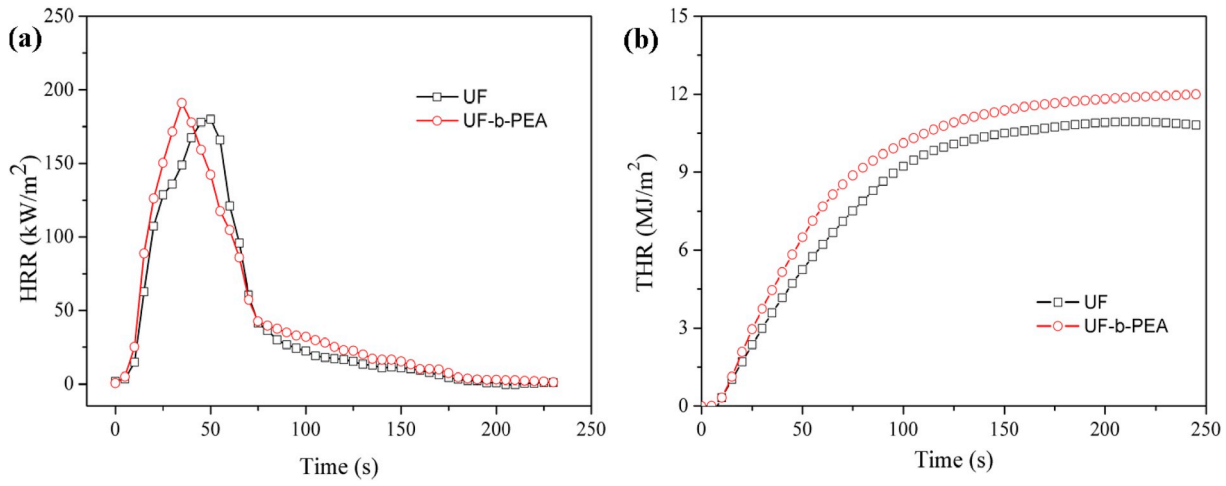

Fig. 13. Heat release rate and total heat release curves of neat UF and UF-b-PEA foam.

at weak or defective sites, resulting in an permanent deformation as shown as ③*. Such irreversible damage zone could be observed clearly from the SEM image of neat UF foam during compression in this stage. For configuration ④, UF-b-PEA foam still had good elastic resilience when unloading due to the less fracture of the cell strut. As shown as the SEM image of UF-b-PEA foam, no obvious damage can be observed in this stage.

3.4. Flammability properties of UF-b-PEA foam

To evaluate the flammability, limiting oxygen index (LOI) and vertical burning UL-94 tests for UF foam and UF-b-PEA foams were measured, and the results were presented in Table 2. It can be noted that, the LOI values decreased with the increase of PEA content. However, the LOI values maintained above 30%. The UL-94 tests were classed as a V-0 rating for all samples of UF-b-PEA foam, indicating outstanding flame retardancy for the foams. Fig. 12 showed the photographs of foams after UL-94 test. It can be seen that the compact char layer formed for all foam samples, which can suppress the expansion of the flame during burning.

Cone calorimeter measurement was believed to be one of the most effective methods for assessing the fire behavior of materials, from which parameters such as heat release rate (HRR), the peak of HRR (PHRR) and total heat release (THR) can be obtained. As shown in Fig. 13, both UF foam and UF-b-PEA foam revealed similar characteristics of thermally thickening charring, for which an initial increase in HRR appeared until an efficient char layer formed and then the char layer thickened resulting in a decrease in HRR. For neat UF foam, the HRR reached the peak value of 179.3 kW/m^2 in 50s, while, for UF-b-PEA foam, the peak value increased slightly. Moreover, the value of THR for neat UF and UF-b-PEA foam were 10.8 MJ/m^2 and 11.9 MJ/m^2 in 250 s, respectively. Therefore, it can be concluded that, incorporation of PEA into UF system showed a negligible effect on the flame retardant properties of the foam product.

4. Conclusion

A serious of UF-b-PEA foams with ultra-elasticity and intrinsic flame retardancy were fabricated. During the synthesis process, PEA molecules were successfully introduced onto the UF molecular chains through the reactions of PEA involved hydroxymethylation and condensation in UF system. The curing process of UF-b-PEA proceeded within a broader temperature ranges, and the peak temperature shifted to a higher temperature. With the increase of PEA content, the apparent density decreased, while the cell size, strut length and open cell porosity increased. During the cyclic compression, the Mullins effect and the area in the hysteresis loop of the UF-b-15 wt%PEA foam were reduced obviously, indicating the outstanding compression resilience and compressive stability of the foam. For UF-b-PEA foams, the F_c decreased and the deformation of the single cell became easier, resulting in the occurrence of large cooperative deformation of cells. For all UF-b-PEA foams, the LOI values maintained above 30% and UL-94 tests were classed as a V-0 rating, while introduction of PEA showed a negligible effect on the value of PHRR and THR of the foam during cone calorimeter measurement, indicating outstanding flame retardancy.

Acknowledgements

This study was financially supported by the Joint Fund of National Natural Science Foundation of China and China Academy of Engineering Physics (NSAF) (Grant No. U1530144).

References

[1] Singha AS, Thakur VK. Synthesis and characterization of short Grewia optiva fiber-based polymer composites. Polym Compos 2010;31:459–70.
[2] Wu BY, Ye L, Liu YL, Zhao XW. Intercalation structure and toughening mechanism of graphene/urea-formaldehyde nanocomposites prepared via in situ polymerization. Polym Int 2018;67:330–9.
[3] Park BD, Roh K. Effects of formaldehyde/urea mole ratio and melamine content on the hydrolytic stability of cured urea-melamine-formaldehyde resin. Eur J Wood Wood Prod. 2009;67:121–3.
[4] Costa N, Pereira J, Martins J. Alternative to latent catalysts for curing UF resins used in the production of low formaldehyde emission wood-based panels. Int J Adhesion Adhes 2012;33:56–60.
[5] Braun D, Guenther P. Studies on the morphological characterization of urea-formaldehyde-foams. J Cell Plast 1985;21:171–7.
[6] Ren Y, Yuan D, Li W. Flame retardant efficiency of KH-550 modified urea-formaldehyde resin cooperating with ammonium polyphosphate on polypropylene. Polym Degrad Stab 2018;151:160–71.
[7] Liu DY, Zhao B, Wang JS. Flame retardation and thermal stability of novel phosphoramide/expandable graphite in rigid polyurethane foam. J Appl Polym Sci 2018;27:135–45.
[8] Otto GP, Moisés MP, Carvalho G. Mechanical properties of a polyurethane hybrid composite with natural lignocellulosic fibers. Compos B Eng 2017;110:459–65.
[9] Gaan S, Liang S, Mispreuve H. Flame retardant flexible polyurethane foams from novel DOPO-phosphonamidate additives. Polym Degrad Stab 2015;113:180–8.
[10] Jiang L, Xiao H, Zhou Y. Theoretical and experimental study of width effects on horizontal flame spread over extruded and expanded polystyrene foam surfaces. J Fire Sci 2014;32:193–209.
[11] Kaji K, Yoshizawa I, Kohara C. Preparation of flame-retardant polyethylene foam of open-cell type by radiation grafting of vinyl phosphonate oligomer. J Appl Polym Sci 1994;51:841–53.
[12] Shahapurkar K, Garcia CD, Doddamani M. Compressive behavior of cenosphere/epoxy syntactic foams in arctic conditions. Compos B Eng 2018;135:253–62.
[13] Hu X, Cheng W, Li C. Effects of surfactants on the mechanical properties, microstructure, and flame resistance of phenol-urea-formaldehyde foam. Polym Bull 2016;73:1–20.
[14] Li Q, Chen L, Zhang J. Enhanced mechanical properties, thermal stability of phenolic-formaldehyde foam/silica nanocomposites via in situ polymerization. Polym Eng Sci 2015;55:2783–93.

[15] Jayavardhan ML, Kumar B, Doddamani M. Development of glass microballoon/HDPE syntactic foams by compression molding. Compos B Eng 2017;130:119–31.
[16] Hu X, Cheng W, Nie W. Flame retardant, thermal, and mechanical properties of glass fiber/nanoclay reinforced phenol-urea-formaldehyde foam. Polym Compos 2016;37:2323–32.
[17] Pinto G, Maaroufi AK. Nonlinear electrical conductivity of tin-filled urea-formaldehyde-cellulose composites. Polym Compos 2005;25:401–6.
[18] Despres A, Pizzi A. Colloidal aggregation of aminoplastic polycondensation resins: urea-formaldehyde versus melamine-formaldehyde and melamine-urea-formaldehyde resins. J Appl Polym Sci 2006;100:1406–12.
[19] Liu J, Nan JY, Wang CP. Modification research of cellulose based urea-formaldehyde resin molding compound. J Nanjing For Univ (Nat Sci Ed): Nat Sci Educ 2015;39:127–31.
[20] Han CG, Li SH. Effects of different plasticizers on performance of urea formaldehyde molding plastics. Mod Chem Ind 2011;31:61–5.
[21] Yuan JL, Zhao XW, Ye L. Structure and properties of urea-formaldehyde resin/polyurethane blend prepared via in-situ polymerization. RSC Adv 2015;5:53700–7.
[22] Liu YL, Zhao XW, Ye L. A novel elastic urea-melamine-formaldehyde foam: structure and properties. Ind Eng Chem Res 2016;55:8743–50.
[23] Petrov P, Jankova K, Mateva R. Polyamide-6-b-polybutadiene block copolymers: synthesis and properties. J Appl Polym Sci 2003;89:711–7.
[24] Xu S, Ye L. Monomer casting nylon-6-b-polyether amine copolymers: synthesis and properties. Compos B Eng 2015;79:170–81.
[25] Xiang M, Xu S, Li C. Monomer casting nylon-6-b-polyether amine copolymers: synthesis and antistatic property. Polym Eng Sci 2016;56:817–28.
[26] Dhakate SR, Subhedar KM, Singh BP. Polymer nanocomposite foam filled with carbon nanomaterials as an efficient electromagnetic interference shielding material. RSC Adv 2015;5:43036–57.
[27] Gong R, Xu Q, Chu Y. A simple preparation method and characterization of epoxy reinforced microporous phenolic open-cell sound absorbent foam. RSC Adv 2015;5:68003–13.
[28] Zou J, Chen Y, Liang M. Effect of hard segments on the thermal and mechanical properties of water blown semi-rigid polyurethane foams. J Polym Res 2015;22:120–30.
[29] Xue B, Li R, Deng J. Sound absorption properties of microporous poly (vinyl formal) foams prepared by a two-step acetalization method. Ind Eng Chem Res 2016;55:3982–9.
[30] Yu Q, Zhao Y, Dong A. Mechanical properties of EPS filled syntactic foams prepared by VARTM. Compos B Eng 2018;136:126–34.
[31] Wu N, Xiu Z. Surface microencapsulation modification of aluminum hypophosphite and improved flame retardancy and mechanical properties of flame-retardant acrylonitrile-butadiene-styrene composites. RSC Adv 2015;15:49143–52.
[32] Cheng Y, Li J, He Y. Acidic buffer mechanism of cyclotriphosphazene and melamine cyanurate synergism system flame retardant epoxy resin. Polym Eng Sci 2015;15:1046–51.
[33] Park BD, Jeong HW. Hydrolytic stability and crystallinity of cured urea–formaldehyde resin adhesives with different formaldehyde/urea mole ratios. Int J Adhesion Adhes 2011;31:524–9.
[34] Samaržija-Jovanović S, Jovanović V, Konstantinović S. Thermal behavior of modified urea–formaldehyde resins. J Therm Anal Calorim 2011;104:1159–66.
[35] Zorba T, Papadopoulou E, Hatjiissaak A. Urea-formaldehyde resins characterized by thermal analysis and FTIR method. J Therm Anal Calorim 2008;92:29–33.
[36] Gong L, Kyriakides S, Jang WY. Compressive response of open-cell foams. Part I: morphology and elastic properties. Int J Solids Struct 2005;42:1355–79.
[37] Gaitanaros S, Kyriakides S. On the effect of relative density on the crushing and energy absorption of open-cell foams under impact. Int J Impact Eng 2015;82:3–13.
[38] Zhu HX, Mills NJ, Knott JF. Analysis of the high strain compression of open-cell foams. J Mech Phys Solids 1997;45:1875–904.